CLIMATOLOGY

Should we think of observationally constrained multidecade climate projections as predictions?

Tong Li[1], Francis W. Zwiers[1,2]*, Xuebin Zhang[1]

Empirical evidence indicates that the range of model-projected future warming can be successfully narrowed by conditioning the projected warming on past observed warming. We demonstrate that warming projections conditioned on the entire instrumental annual surface temperature record are of sufficiently high quality and should be considered as long-term predictions rather than merely as projections. We support this view by considering the skill of predicted 20- and 50-year lead temperature changes under the Shared Economic Pathway (SSP)1-2.6 and SSP5-8.5 emission scenarios in climates of different sensitivities. Using climate model simulations, we show that adjusting raw multimodel projections of future warming with the Kriging for Climate Change (KCC) method eliminates most biases and reduces the uncertainty of warming projections irrespective of the sensitivity of the climate being considered. Simpler methods, or using only the more recent part of the temperature record, provide less effective constraints. The high-skill future warming predictions obtained via KCC have a serious place in informing global climate policies.

INTRODUCTION

Human-induced climate change is causing widespread increases in climate risks (*1*–*3*) that can be partially mitigated through improved predictions of long-term climate change (*4*, *5*). For example, more precise information about the future state of the climate would enable engineers to design infrastructure that meets resilience requirements during its expected service life at a lower cost (*6*).

Climate projections are made with climate models that are typically initialized from a long preindustrial simulation and then integrated forward in time accounting only for estimated historical external forcings and future forcing scenarios (*7*, *8*). These projections are subject to large modeling uncertainty and cannot be verified against the yet-to-be-observed future. Previously made multimodel projections of near-term warming have been assessed relative to recent observations and have proven to be generally successful, but their evaluation against observations also demonstrates the difficulties that arise because of modeling uncertainty and the large influence of internal variability in the near term (*9*–*13*).

Early studies that used observations to constrain future projections (*14*–*16*) did so without considering statistical relationships between past and future states simulated by climate models. Improved statistical tools that consider observed and model-simulated historical changes together with model-simulated future changes [also known as emergent constraints (ECs)] have enabled improved observationally constrained model projections. Many of these studies have used observed changes since 1980 as a constraint (*17*–*19*), as this period has been less affected by changes in aerosol forcing than earlier periods (*17*, *20*–*22*). This has successfully narrowed modeling uncertainty under a given emission scenario (*17*, *23*–*25*). Earlier studies used linear regression models to constrain equilibrium climate sensitivity (*26*–*28*) and snow albedo feedback (*29*, *30*). Recent studies have also used Bayesian-based methods, including hierarchical emergent constraints (HECs) (*31*) and Kriging for Climate Change (KCC) (*25*), to constrain future projections of extreme precipitation (*18*, *32*) and regional and global mean temperatures (*25*, *33*–*35*).

Climate predictions on timescales of a season up to a decade are made with climate models that are initialized with the current observed climate state and use prescriptions of the historical and near-term future external forcing (*36*). That is, climate prediction describes a future evolution of the state of the Earth system that is conditional on a recently observed state and some specified boundary conditions. ECs operate by making a projected change conditional on past, observed climate change and work when the future evolution of the climate depends on how the climate has attained its current state (*37*, *38*). Thus, the problem addressed by constrained climate projections is not so different from that of climate prediction. While long-term climate projections by climate models are not initialized, ECs make it possible to frame the projection problem much more confidently as a prediction problem, where future outcomes are understood as being conditional on present and past conditions and some assumed boundary conditions in the form of an emissions path.

Making predictions of future change conditional on observed historical changes naturally leads us to consider the Bayesian-based approach in this study and, thus, either the HEC or KCC methods. These methods are conceptually identical, with differences between various studies being due to implementation choices. In all cases, the idea is to use multimodel projections to obtain a prior distribution on a projected future change that is then updated with evidence from past observations to produce a posterior distribution on that future change that is both narrower and hopefully more closely centered on the future truth. This understanding, along with the availability of large ensemble simulations by climate models of different sensitivities, enables us to investigate the sources and level of skill in multidecade climate predictions. We focus on predicting the climate of future 20-year periods relative to the current climate (1994–2023) with 20- and 50-year lead times, as these time frames are highly relevant for adaptation planning and mitigating climate risk (*39*). We demonstrate that the evolution of historical global mean temperature to date contains sufficient information to produce predictions

[1]Pacific Climate Impacts Consortium, University of Victoria, Victoria, BC, Canada. [2]Key Laboratory of Meteorological Disaster, Ministry of Education, Collaborative Innovation Center on Forecast and Evaluation of Meteorological Disasters, Nanjing University of Information Science & Technology, Nanjing, China.
*Corresponding author. Email: fwzwiers@uvic.ca

that have substantially lower bias and uncertainty than unconstrained multimodel projections.

RESULTS

EC performance

The EC problem is essentially a missing data problem. Models provide simulations of historical and future states, but observations can only provide us with estimates of past climate states. ECs aim to estimate the "missing" future observations using past observations and climate models. To test EC performance, individual climate model simulations can be used as pseudo-observations, which, unlike real observations, are available for both the past and future states. This allows ECs in different configurations to be repeatedly applied to different realizations of pseudo-observations of the past, with the resulting constrained projections being verified against corresponding future pseudo-observations. Using climate models with different characteristics, including different climate sensitivities, we can determine whether an EC will also perform well when using the particular realization of the observed climate system that we are experiencing and assess the skill of constrained future projections when treated as predictions (see Materials and Methods for details). Specifically, we use individual simulations from three climate models, the Model for Interdisciplinary Research on Climate version 6 (MIROC6) (40), the Australian Community Climate and Earth System Simulator Earth System Model version 1.5 (ACCESS-ESM1.5) (41), and the Canadian Earth System Model version 5 (CanESM5) (42) with large ensemble simulations that have low, medium, and high sensitivities among all Coupled Model Intercomparison Project Phase 6 (CMIP6) models as pseudo-observations. These represent cases where the projected warming is substantially lower than, similar to, or greater than the multimodel mean warming of the remaining CMIP6 models that are used to predict the future state.

Results show that the use of the year-by-year temperature evolution during the preindustrial period (1851–1900) does not allow KCC to produce useful constraints; the bias in projected temperature over a 50-year lead time is not reduced (Fig. 1A), and projection uncertainty remains similar to the raw model projection uncertainty (Fig. 1B). This outcome is expected because external forcing during this period is too weak to produce a detectable response in global mean surface temperature (43). As we will also discuss later, good performance, in terms of reducing bias and narrowing projection uncertainty, only becomes possible when the transient response to anthropogenic forcing becomes detectable.

The best estimates of projections constrained by the global mean surface temperature evolution over periods of different lengths ending in 2023 align well with future changes in the pseudo-observations under the Shared Socioeconomic Pathway (SSP)5-8.5 scenario, despite large biases in the raw multimodel mean projections relative to the "reality" of the pseudo-observations from either MIROC6 or CanESM5 (Fig. 1A). Using periods that contain information about the transient response of the climate to forcing provides KCC with sufficient information to effectively adjust for bias in the model-projected warming spanning the range of climate sensitivities in the CMIP6 cohort of models, even when considering constraint periods beginning as recently as 1981 (Fig. 1A). Similar results are obtained under the SSP1-2.6 scenario (fig. S1A), although under this scenario, temperature stabilizes at a new, warmer level in the second half of the 21st century. This is consistent with the notion that the transient

response to forcing during the observational period is key to constraining future temperatures via KCC and that the new stabilized temperature is mainly the result of the warming during a period of strong transient response.

Conditioning on the specific realization of historical climate over a period that includes the past few decades substantially reduces model uncertainty in estimating future change, even when the bias in the unconstrained multimodel projection is essentially zero (Fig. 1B). Furthermore, using a period that includes the full transition from a quasiequilibrium preindustrial state to the recent strong transient response leads to a better constraint under both the high-emission scenario SSP5-8.5 and the low-emission scenario SSP1-2.6 (Fig. 1B and fig. S1B). For instance, when simulations from CanESM5 are used as pseudo-observations, constraining model projections using the 1851–2023 period narrows the uncertainty range by about 55% (1.48° and 0.76°C under the SSP5-8.5 and SSP1-2.6 scenarios, respectively) compared to the unconstrained projections. In contrast, constraining projections with the commonly used 1981 to present period (17, 44) only reduces the uncertainty range by about 30% [0.99°C (36%) and 0.58°C (43%), respectively, under SSP5-8.5 and SSP1-2.6]. Under the SSP5-8.5 scenario, 92% of predictions from the individual runs of a given large ensemble fall within the 5 to 95% uncertainty range of the constrained projection, indicating no evidence of overconfidence (fig. S2).

While much improved relative to unconstrained projections, the constrained projections do continue to exhibit substantial uncertainty (Figs. 1A and 2 and fig. S3). The 5th to 95th percentile variation in best estimates of prediction with a 50-year lead time under the SSP5-8.5 emission scenario can exceed 1°C when constrained by pseudo-observed warming up to 2023. This uncertainty originates from the natural variability of the pseudo-observations during the historical constraint period, as the forcing response signal-to-noise ratio is necessarily lower during the constraint period than during the future response period that is of primary interest. One indication of the effect of internal variability during the observational constraint period is that differences between individual realizations of historical pseudo-observations affect the predictions of future change as can be seen when constrained projected change is plotted against pseudo-observed warming trends (Fig. 2 and fig. S3). Stronger warming is predicted when the historical trend is larger in the pseudo-observations used in the constraining relation, while future warming remains similar regardless of the magnitude of trends in the historical period within the same time series of pseudo-observations. This indicates that while multidecadal low-frequency variability in the historical period may provide some predictive skill with a lead time of a decade or two (45), it does not do so for longer lead times. This means that while ongoing research may be able to reduce model uncertainty, the accuracy of the best estimate of future change constrained by the single observed evolution of warming that is available for the real world remains limited by the influence of internal variability on the observed evolution, which is not considered to be predictable for the long-term future. The influence of this source of uncertainty will slowly decline, as the observational record continues to lengthen and the response to forcing continues to further dominate the change seen in the observational record. Improved techniques that separate key aspects of natural variability in the observations from the externally forced component of change (46) will also help to further reduce uncertainty in constrained estimates of future warming due to external forcing.
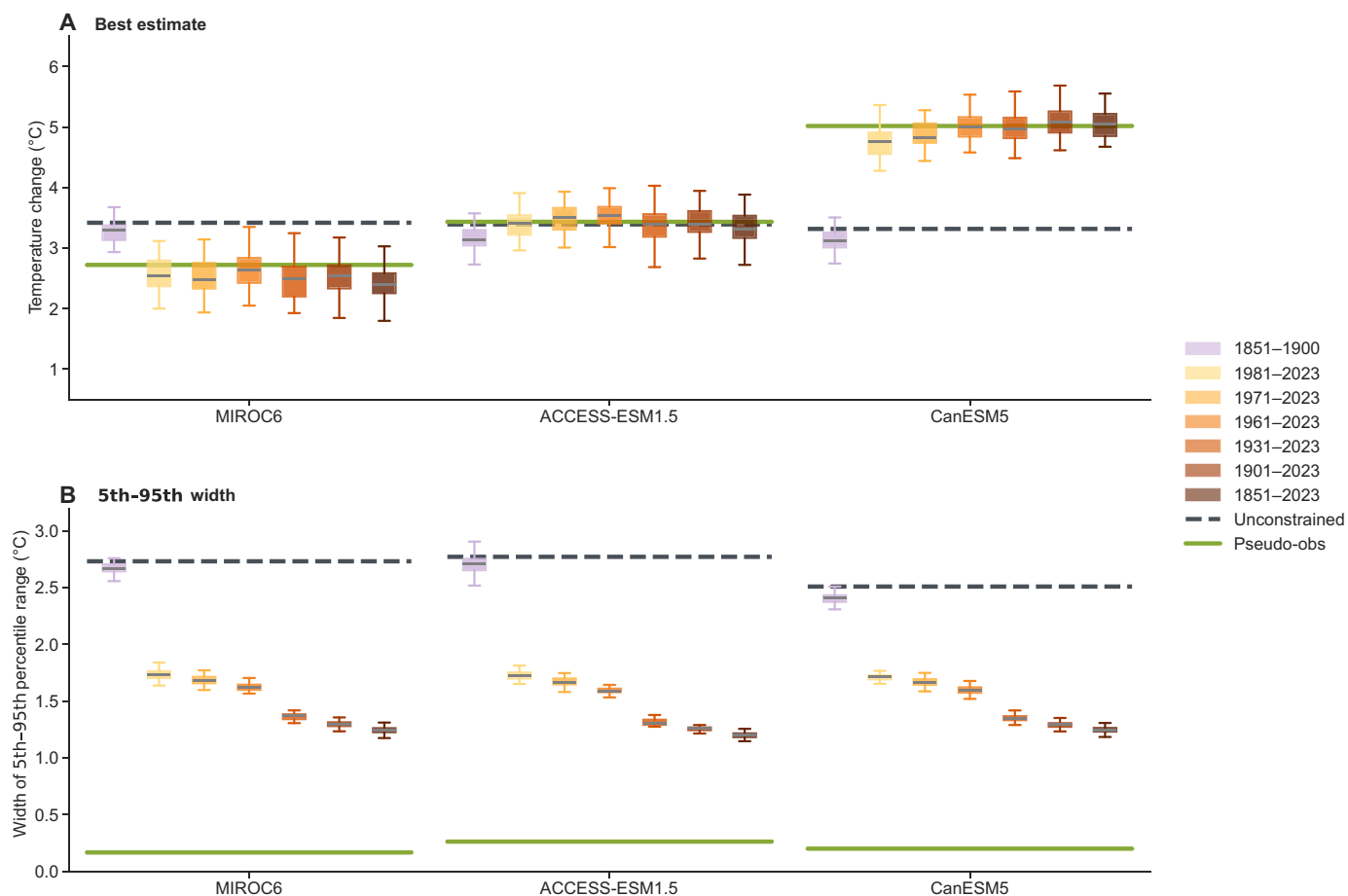
Fig. 1. Observational constraints with the KCC method can effectively reduce bias and model uncertainty in multimodel projections. (**A**) shows box plots of the best estimates of prediction (constrained projections) for global mean surface temperature for the future 20-year period (2074–2093) at a 50-year lead time relative to current climate conditions (1994–2023) when individual model runs are used as pseudo-observations to establish the constraining relation. These projections are conditional on historical temperature changes during different periods in pseudo-observations (Pseudo-obs) from individual MIROC6, ACCESS-ESM1.5, and CanESM5 simulations under the SSP5-8.5 emission scenario (table S1). The results for different constraint periods are represented by box plots, with the 1851–1900 preindustrial period shown in purple and other periods in varying shades of orange. The green lines depict the projected changes of the large ensemble means, while the black dashed lines show the mean value of raw multimodel projections. (**B**) shows box plots of the associated widths of the 5th to 95th percentile ranges of the predictions calculated from the 90% confidence intervals. Green lines depict the spread of the 5th to 95th percentile by the large ensembles, while gray lines indicate the multimodel spread. The green line represents uncertainty due to internal variability specific to each model, and thus, it represents the minimum uncertainty that would be achievable in the complete absence of model uncertainty. The spread of the box plots shows the differences due to internal variability among results for individual runs. The tick marks in the box plots indicate the median value, the boxes show the interquartile range (IQR), and the whiskers extend to 1.5 × IQR. The 1851–1900 period, which does not extend to 2023, has been used to compare constrained projections with periods ending in 2023. See also fig. S1 for the low-emission scenario SSP1-2.6.

Does the observed warming trend provide an adequate observational constraint?

Many recent studies using HEC have used the linear warming trend observed over recent decades, such as 1981–2020, to constrain future projections (*32*, *47*, *48*). Arguments (*17*, *18*) that justify this choice focus on the roughly linear increase in greenhouse gas forcing and the roughly constant level of other anthropogenic forcing effects over this period (*23*), which together lead to the expectation of a linear warming response during this period. Using the linear warming trend over recent decades does improve upon unconstrained projections but to a lesser extent than when using all available evolution information during the same periods (blue boxes versus red boxes in Fig. 3 and figs. S4 to S6). In addition, bias in trend-based constrained projections can be sensitive to the selection of time periods from which trends are estimated.

The lowest bias in the constrained projection of future warming is achieved when the trend is computed from a longer period starting between 1931 and 1961, although a linear trend does not fully describe temperature change over periods starting this early. Similarly, conditional uncertainties are lowest when considering a trend that starts between 1931 and 1961. Trends computed over shorter periods, where a linear trend more accurately represents changes in global mean surface temperature over the periods, are able to provide useful constraints and reduce uncertainty in future projections (*17*, *24*) but are more sensitive to trend uncertainty due to internal variability. On the other hand, trends computed from a longer period starting before 1931 are less effective because they provide only small bias and conditional uncertainty reductions compared to unconstrained projections, possibly due to the poor fit of the trend line to the temperature series in these cases.
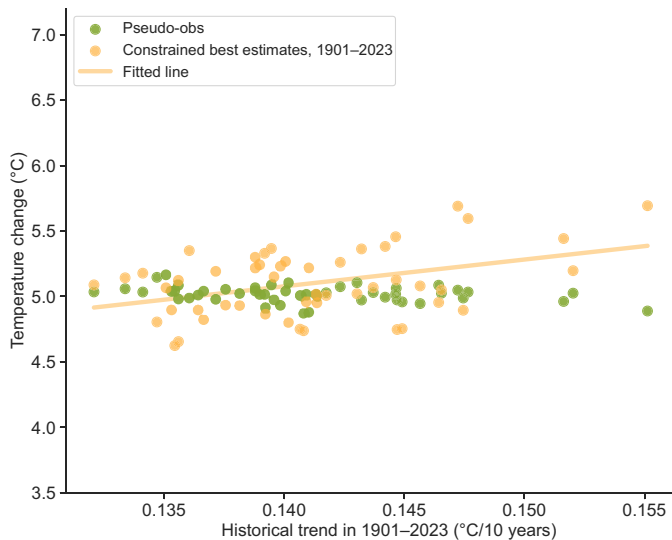
Fig. 2. Natural variability in the observation can affect observation-constrained projections. Projected changes in global mean temperature from pseudo-observations (individual runs of a large ensemble, green dots) and the corresponding constrained projections using a 1901–2023 constraint period (based on individual runs of a large ensemble, orange dots) for the future 20-year period (2074–2093) at a 50-year lead time relative to the current climate condition (1994–2023). The projections are plotted with the *x* axis representing the historical trend of pseudo-observations during 1901–2023 in ascending order. The fitted regression line is shown in yellow. While model-projected future temperature changes in pseudo-observations are not affected by past warming in the same pseudo-observation, constrained future projections are affected by the past warming trend. This figure presents results for pseudo-observations simulated by CanESM5 under the SSP5-8.5 scenario. See also fig. S3 for results for pseudo-observations simulated by ACCESS-ESM1.5 and MIROC6 (unit: °C).

Fitting a linear trend to the historical observations requires estimating an intercept parameter, even if not used. As we are using temperature anomalies relative to the preindustrial period, the intercept term provides information on the cumulative warming that occurred since that preindustrial baseline, before the constraining period. This is confirmed by the nearly 1-1 relationship in fig. S7. Using both the trend and intercept estimates to constrain future projections generally improves upon projections constrained only by the observed trend (orange boxes versus blue boxes in Fig. 3 and figs. S4 to S6), bringing the bias and conditional uncertainty closer to that obtained when using all information (as in KCC), although it still does not fully match KCC's effectiveness (orange boxes versus red boxes in Fig. 3 and figs. S4 to S6). The improvement in bias reduction can be seen particularly in the more recent period when compared to the earlier period. This is because over time, the accumulated warming increases, thereby amplifying the importance of the intercept in the constraining future projection. The warming between the preindustrial period and the constraint period is greater for models in which surface temperature begins to warm more quickly after the start of the industrial period. This response depends largely on the proportion of absorbed incoming solar energy used to change the ocean's heat content and the temperature needed to radiate unabsorbed heat back to space (*49–51*).

Origins of the information that provide the constraint

The posterior distribution (Eqs. 6 and 7) for the projected warming offers insights into the sources of skill in constraining projections. In simplified terms, the posterior distribution is obtained by adjusting the prior distribution to account for the difference between the observed historical change and the multimodel mean–simulated historical change. This adjustment is based on three key factors: (i) the difference ($\mathbf{Y}_o - \mathbf{X}_h$) between the historical observations expressed as anomalies relative to a fixed base period and the multimodel mean simulation of those historical changes, (ii) the cross-covariance between model historical simulations and future projections ($\mathbf{\Sigma}_{x_f x_h}$), and (iii) the combined uncertainty in the historical model simulations and observations ($\mathbf{\Sigma}_{x_h x_h} + \mathbf{\Sigma}_o$).

For the best estimate of the constrained projection, the first term influences both the direction and magnitude of the adjustment needed to account for the difference between the global mean surface temperature evolution in the climate of the model providing the pseudo-observations and that in the remaining CMIP6 ensemble (Fig. 4A). The magnitude of this adjustment is controlled by the combined uncertainty in simulated and observed historical values and the strength of the relationship between past and future values in the model. A larger uncertainty in the historical period reduces the magnitude of the adjustment, while a larger cross-covariance matrix $\mathbf{\Sigma}_{x_f x_h}$, indicating a strong relationship between historical and future global mean surface temperature values in the model simulations (Fig. 4B), increases the magnitude of the adjustment. Note that there is no adjustment to the unconstrained multimodel projections when the cross-covariance is zero. Larger cross-covariance values connecting future values to historical values tend to emerge more prominently in recent decades after 1990, coinciding with the period when the warming signal becomes more evident [figure 1.14 in the Intergovernmental Panel on Climate Change (IPCC) (*3*)]. Because of this high correlation, the information from the period after 1990 is particularly important in determining the effectiveness of future constraints. The consistently positive constraint effects of each constraining period shown in Fig. 1 result from incorporating this period into the analysis. As will be discussed later, excluding information from the recent period of rapid transient change generally weakens the effectiveness of the constraint (Fig. 5 and fig. S8).

An empirical orthogonal function (EOF) analysis of the intermodel differences, as represented in covariance matrix $\mathbf{\Sigma}_{x_h x_h}$, helps to highlight the sources of uncertainty that limit the influence of the historical observed changes on the posterior distribution of future temperature change. Except for the preindustrial-only period, the first EOF (EOF1) shows a pattern of secular global mean surface temperature change over time that indicates how the cumulative warming response to forcing varies between models, with larger variation in recent decades than in earlier decades. This EOF accounts for more than 69% of the total intermodel variance (Fig. 4C). The second EOF (EOF2) can be interpreted as representing variations in smoothed non–greenhouse gas forcing response between models (Fig. 4D). Models showing a stronger non–greenhouse gas influence, which is dominated by aerosols (*23*), during the early and mid–20th century show faster warming in recent decades when aerosol has been roughly stable. However, second- and higher-order EOFs are inherently more difficult to interpret because of the orthogonality constraint that is imposed by EOF analysis. Together, these two EOFs account for more than 96% of the variance in the recent rapid transient warming periods post-1961. Note that when incorporating $\mathbf{\Sigma}_o$ into the EOF analysis, the leading EOF1 and EOF2 patterns remain identical but explain slightly less of the total variance. When the global mean surface temperature time series starts before
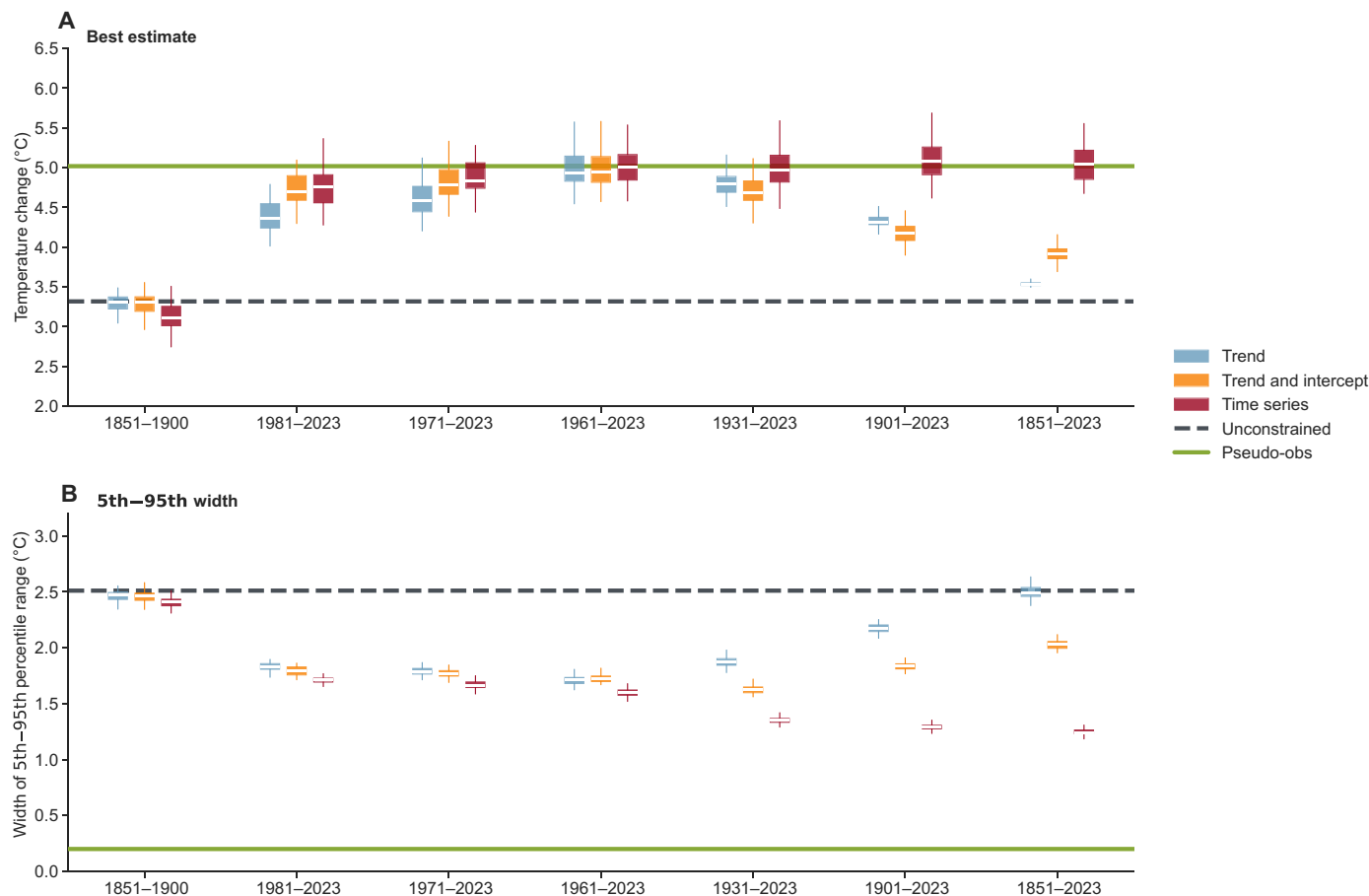
Fig. 3. Using more information from the historical record improves constrained projections. Same as Fig. 1, (**A**) best estimates of prediction (constrained projections) and (**B**) the associated width of 5 to 95% confidence intervals for global mean surface temperature for the future 20-year period (2074–2093) at a 50-year lead time relative to the current climate condition (1994–2023). These projections are conditional on historical temperature trend (blue), trend and intercept (orange), and time series (red) during different periods in pseudo-observations from CanESM5 simulations under the SSP5-8.5 emission scenario. Green and black dashed lines depict mean values for the large ensemble of pseudo-observations and raw multimodel projections, respectively. The results constrained by the full time series are identical to those for CanESM5 pseudo-observations in Fig. 1. See also figs. S4 and S5 for results from pseudo-observations simulated by ACCESS-ESM1.5 and MIROC6.

1960 and thus includes a period of smaller climate response, the leading two EOFs account for less than 83% of the total variance, indicating a more complex combination of uncertainties that affect the strength of the constraint on projections of future warming. KCC, which uses all available information, successfully addresses this complexity, producing the greatest uncertainty reductions when the observational constraint includes both recent and early warming parts of the record. In contrast, a simple linear model that includes a trend term and possibly an intercept term, extracting at most the equivalent of the information carried by EOFs 1 and 2, relies exclusively on the aspects of the warming of the Earth system that contribute most strongly to intermodel variation in the simulation of historical change.

Constrained projections should be considered to be long-term climate predictions

Although model uncertainty remains large, the substantial improvement obtained by using KCC in pseudo-observed climates of different climate sensitivities makes it possible to interpret the resulting constrained projections as predictions that, in the medium to long

term, are conditional on the chosen emissions pathway. To demonstrate the substantial predictive skill of the constrained projections and how it improves with the inclusion of more historical data, we compare the root mean square error (RMSE; Fig. 5A and fig. S8) between the predicted changes and the changes in the verifying pseudo-observations during a future 20-year period relative to the climate of the last 30 years of the constraining period, with lead times of 20 and 50 years. This comparison involves pseudo-observations from the three large ensembles, with observations ending at the time of past IPCC assessments and the upcoming seventh assessment and second global stocktake.

While the constrained projections show some skill even at the time of the IPCC's first and second assessments, there is clear evidence of skill across pseudo-observations from all three large ensembles starting at the time of the IPCC's third assessment (~2000) when the IPCC stated that "most of the observed warming over the last 50 years is *likely* to have been due to the increase in greenhouse gas concentrations" (*52*). Predictions with shorter lead times exhibit better skill, as indicated by smaller RMSE values. The RMSEs decrease to around 0.15°C for the 20-year lead time and to 0.3°C for
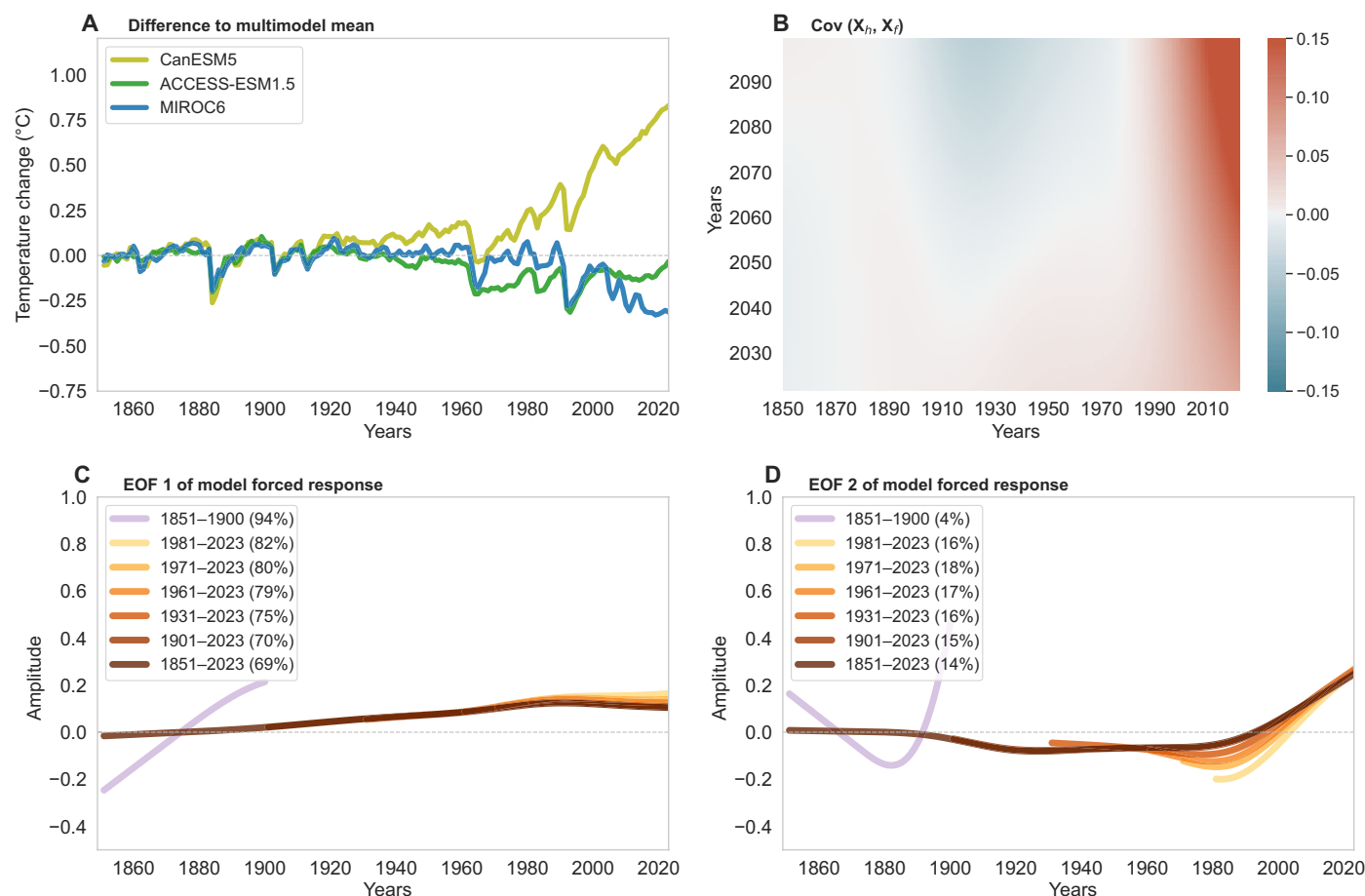
Fig. 4. The response to external forcing in climate model simulations, along with the differences in model responses, can be represented in relatively few dimensions but is nevertheless difficult to approximate with simple functions. (**A**) Difference between ensemble mean responses of the three large ensembles and the mean response from CMIP6 models to historical external forcings. (**B**) Cross-covariance matrix between historical and future periods in smoothed CMIP6 simulations. (**C** and **D**) The first and second EOFs (empirical orthogonal functions) of the historical simulations of smoothed CMIP6 models.

the 50-year lead time under the SSP5-8.5 scenario when simulations by the mid-sensitivity model ACCESS-ESM1.5 are used as pseudo-observations. Larger improvements in the prediction accuracy over CMIP6 raw projection are associated with pseudo-observations simulated by the low and high climate sensitivity models, again indicating the effectiveness of observational constraint in reducing model bias (fig. S8).

On the basis of the available historical record, we predict (Fig. 5B) that the 2044–2063 global mean temperature (20-year lead time) will be 0.8°C [0.6°C, 1.1°C] warmer than the 1994–2023 mean under the SSP1-2.6 scenario and 1.5°C [1.2°C, 1.8°C] warmer under the SSP5-8.5 scenario. Note that with the large reduction in modeling uncertainty, the 90% ranges of the warming predictions conditional on these two scenarios do not overlap, indicating that a reduction in the rate of global mean warming under SSP1-2.6 should become discernible relative to the warming rate that would have happened under the high emissions of SSP5-8.5 sooner than has generally been anticipated. For example, the IPCC-assessed midterm projections (*3*) for a similar period (2041–2060) indicate warmings of 0.85°C [0.45°C, 1.35°C] (very likely range) and 1.55°C [1.05°C to 2.15°C] relative to 1995–2014 under SSP1-2.6 and SSP5-8.5, respectively. With a lead time of 50 years, we predict that the 2074–2093

global mean temperature will be 0.9°C [0.6°C, 1.2°C] and 3.3°C [2.6°C, 3.9°C] warmer than the 1994–2023 mean under the SSP1-2.6 and SSP5-8.5 scenarios. Comparable IPCC-assessed long-term projections (*3*), which have a comparable nominal lead time, are 0.95°C [0.45°C, 1.55°C] and 3.55°C [2.45°C, 4.85°C], respectively.

DISCUSSION

Simulated changes in future climate under specified external forcing, even those conducted with the most recent Earth system models, continue to be regarded as projections describing the range of plausible outcomes under a specified emission scenario rather than as predictions. In this paper, we argue that the conceptual similarity between observationally constrained projection and climate prediction, the skill of constrained projections in predicting the unobserved future that is evident when using pseudo-observations to provide constraints and verifying future outcomes, and the understanding of the sources of information that provide a skillful constraint support the notion that constrained projections produced with KCC and the full observational global mean surface temperature record should be considered as predictions of expected outcomes under various global climate policies. This provides a unified framework for climate
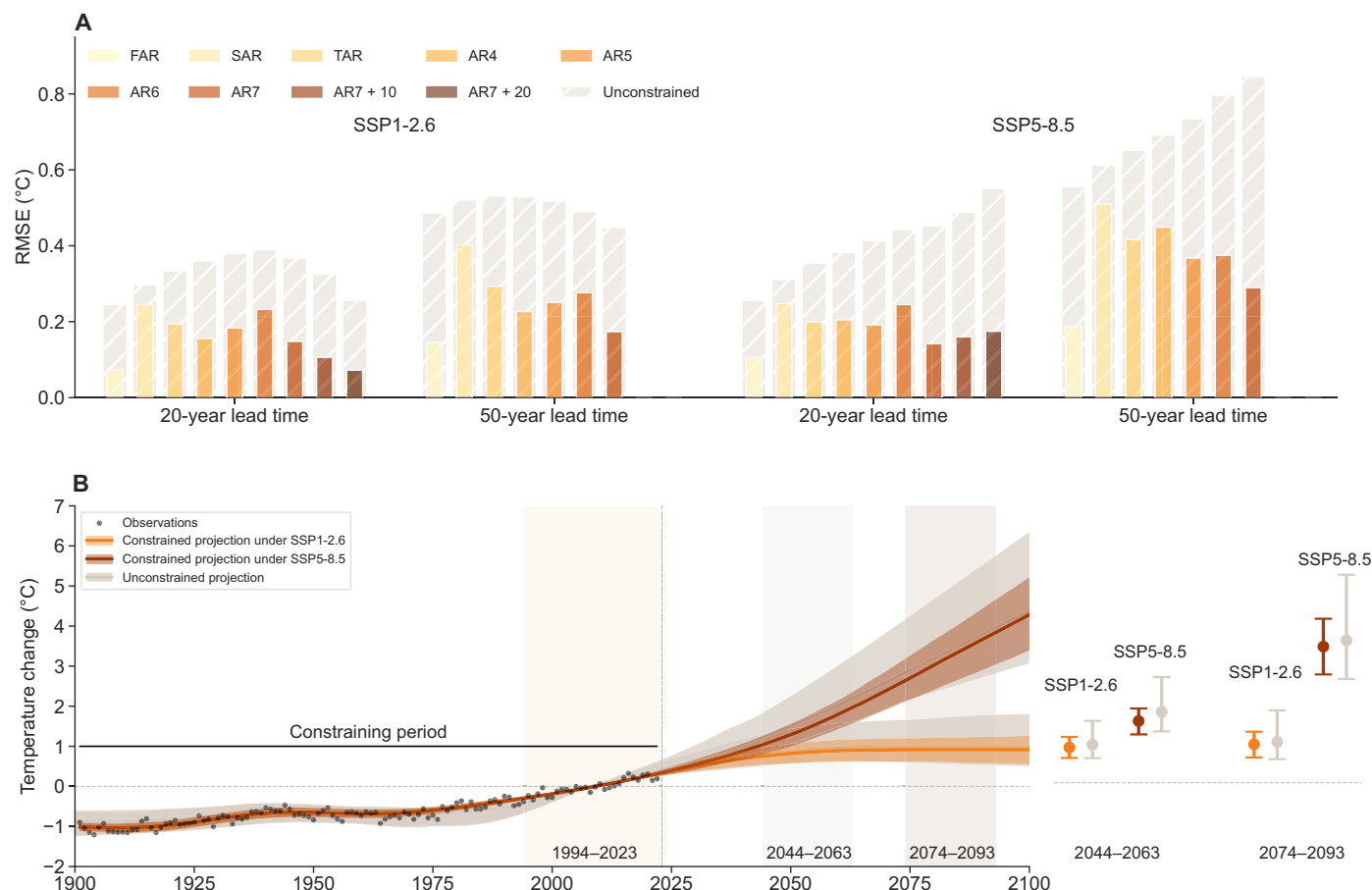
Fig. 5. Predictive skill in the imperfect model world and prediction of global mean surface temperature evolution conditional on time series of annual global mean temperatures from version 5 of the UK Met Office Hadley Centre/Climatic Research Unit (HadCRUT) data set HadCRUT5. (A) The root mean square error (RMSE) of constrained predictions (colored) and unconstrained (gray) relative to pseudo-observations simulated by ACCESS-ESM1.5 during the future 20-year period relative to the current climate (defined as the last 30 years of the constraining window), with lead times of 20 and 50 years under the SSP1-2.6 and SSP5-8.5 emission scenarios. The first year of constraining window is 1901, while the last year corresponds to the year before the release of the IPCC first to seventh assessments [IPCC First Assessment Report (FAR)1990, its Second Assessment Report (SAR) 1995, its Third Assessment Report (TAR) 2000, its 4th Assessment Report (AR5) 2006, its 5th Assessment Report (AR5) 2012, its 6th Assessment Report (AR6) 2020, and its anticipated 7th Assessment Report (AR7) 2026], plus two additional constraining windows that end in 2036 and 2046. ACCESS-ESM1.5 results are shown because it has climate sensitivity similar to the best estimate sensitivity of the observed climate (*62*). **(B)** Historical observations from 1901 to 2023, unconstrained CMIP6 projections, and future predictions. The left panel shows time series, with the predictions in color and unconstrained projections in gray, with their corresponding 5th to 95th percentile ranges shaded. The right panels display warming of the future periods with 20- and 50-year lead time, with mean changes shown as dots and 5th to 95th percentile ranges represented by error bars. The warming relative to the preindustrial period can be determined by applying an offset between 1994–2023 and 1851–1900, which is estimated to be approximately 0.95 [0.89, 1.02] °C based on the HadCRUT5 dataset.

prediction that is suitable for lead times from a season to multiple decades, with future climate being conditional on an observed state of climate and an assumed future evolution of external boundary conditions as embodied in an emissions pathway. The future verifying state of the climate will depend on both the historical evolution of the climate before the time when the prediction is made and the subsequent evolution of the boundary conditions, with predictive skill also being affected by the difference between the assumed boundary conditions and those that will actually occur. While future observations to verify these predictions are not yet available, individual members of large ensemble simulations from models with varying climate sensitivities can be used as pseudo-observations to assess prediction skill. Our evaluation demonstrates superior skill in predicting changes in 20-year mean conditions relative to the recent climate with lead times of 20 and 50 years across different emission scenarios.

The skill of constrained predictions is influenced by methodological and configuration choices in applying ECs. The use of the complete instrumental global mean temperature evolution provides substantially better predictive skill than constraints based only on the linear trend from the recent past. This is because the trend estimation is subject to uncertainty due to internal variability and because trend estimation does not use all of the information in the historical record that is predictive of the future warming response to continued climate forcing. In particular, accounting for the warming that occurred before the period used to provide the constraint contributes to its predictive skill, as do the details of how the Earth system transitioned from a quasistationary preindustrial state to its current rapid transient response state. ECs may not be able to adjust for common errors in forcing across the models if those errors only become apparent under strong future forcing. As we demonstrated,

ECs are only effective when changes in the historical period contain information about changes in the future period, and thus, the constraints may not account for future forcing errors if systematic evidence of such effects is not present in the climate simulations of the historical period.

There are promising opportunities to further improve constrained prediction. One key challenge lies in the unforced internal variability in observations, which can bias the constrained projection. Techniques that identify and separate the dominant patterns of internal variability in observations (46, 53, 54) may lead to more accurate predictions. Incorporating observed variables that more completely represent the physical processes by which heat accumulates in the climate system could further improve constraints and make predictions less sensitive to internal variability (55, 56). Improvements to how we sample from model space that help to improve the estimate of the large variance-covariance matrix representing model uncertainty should also contribute to the more effective use of available historical observations in the constraints. The ability to skillfully predict human-induced climate change decades ahead, based on emissions policies, provides a critical tool for climate adaptation planning and risk management, which should be fully recognized and leveraged.

MATERIALS AND METHODS
Data
Earth system model simulations and observational data
We use climate simulations from models participating in CMIP6 (7), as summarized in table S1, in three different ways:

1) Emergent constraint relations: These are developed using one simulation from each of the CMIP6 models. For each model, we consider the global mean surface temperature change under historical forcing and future emission scenarios SSP1-2.6 and SSP5-8.5. All changes are relative to the 1851–1900 preindustrial levels. Unlike other approaches used in recent research, we use the first run from each model to establish constraining relationship and produce constrained future projections. Doing so ensures that the contribution from each model is similarly affected by internal variability. A detailed discussion of this choice is provided below.

2) Effectiveness evaluation: We evaluate the effectiveness of the constrained projections based on an imperfect model testing procedure (further details below) that uses three large ensemble simulations with different climate sensitivities. These include a 50-member ensemble simulated by CanESM5 [equilibrium climate sensitivity (ECS) of 5.62°C and transient climate response (TCR) of 2.74°C], a 40-member ensemble simulated by ACCESS-ESM1.5 (ECS of 3.87°C and TCR of 1.95°C), and a 50-member ensemble simulated by MIROC6 (ECS of 2.61°C and TCR of 1.55°C). The ECS and TCR values given here are based on table 7.SM.5 of Smith *et al.* (57).

3) Internal variability in observation: Internal variability in the historical observation is estimated using simulations from models listed in table S1 that have more than one ensemble member. Further details are provided below.

The model simulations are first interpolated onto a common 5° × 5° grid, and then the global mean surface temperature changes relative to the preindustrial period are calculated for subsequent analysis. The observed annual global mean surface temperature over the 1850–2023 period is derived from the monthly UK Met Office Hadley Centre/Climatic Research Unit (HadCRUT) data set version HadCRUT.5.0.2.0 values (58). Measurement uncertainty is estimated from the 200 HadCRUT.5.0.2.0 realizations that are available, and the median value of these realizations is taken as the best estimate.

Statistical method
EC method
We constrain future projections using the KCC method (25). Many studies have also used the HEC method (31). These are conceptually similar methods that are both rooted in Bayesian statistics. Below, we will demonstrate that the primary difference between them lies in implementation choices. KCC has been mostly applied in cases where the observable used to provide the constraint is one or more observed time series (25, 34, 35, 59), while HEC has been predominantly used when the constraint is obtained via a scalar observable, such as an observed trend (18, 31, 32).

Both methods treat the constrained projection problem as a missing data imputation problem, where a collection of climate simulations is used to specify a prior distribution on the magnitude of future change for a climate variable of interest. Observations (vectors in the case of KCC or typically a scalar in the case of HEC) are then used to update that prior to produce a posterior distribution. A useful observational constraint results in constrained projections with a narrower distribution than the unconstrained prior and that are more closely centered on the future truth. In both cases, physical arguments underpin the choice of observational constraint.

The statistical model underlying KCC, described in Ribes *et al.* (25) (Eq. 1), can be written as follows in a vector form

$$\text{Observations: } \mathbf{Y}_o = \mathbf{H}\mathbf{Y} + \varepsilon_o, \varepsilon_o \sim \mathrm{N}\left(0, \mathbf{\Sigma}_o\right) \tag{1}$$

$$\text{Model realizations: } \mathbf{X}_i = \mu + \varepsilon_{x,i}, \varepsilon_{x,i} \sim \mathrm{N}\left(0, \mathbf{\Sigma}_x\right) \tag{2}$$

$$\text{Indistinguishability assumption: } \mathbf{Y} \sim \mathbf{X}_i \sim \mathrm{N}\left(\mu, \mathbf{\Sigma}_x\right) \tag{3}$$

where $\mathbf{Y}_o$ is the time series of observations, $\mathbf{Y}$ is the time series representing the historical and future forced response, and $\mathbf{H}$ is an operator matrix $\left[\mathbf{I}_h \ \ 0\right]$ that extracts the part of $\mathbf{Y}$ corresponding to the observational period. The vector ε_o represents random noise associated with internal variability and measurement errors in the observations, which is assumed to follow the Gaussian distribution $\varepsilon_o \sim \mathrm{N}\left(0, \mathbf{\Sigma}_o\right)$. Vector $\mathbf{X}_i$ is a simulation of the historical and future time series from model $i = 1, \ldots, m, \mu$ is the mean over models, and $\varepsilon_{x,i}$ represents noise in the model simulations due to intermodel differences and internal variability, which is also assumed to follow a Gaussian distribution with mean 0 and variance-covariance matrix $\mathbf{\Sigma}_x$. The contribution to $\mathbf{\Sigma}_x$ from internal variability is minimized through temporal smoothing of the model simulations to ensure that $\mathbf{\Sigma}_x$ is strongly dominated by the effects of model uncertainty. The model-observation indistinguishability assumption, as shown in Eq. 3, bridges the observational and model worlds by stating that the forced response in observation $\mathbf{Y}$ is drawn from the same distribution as the model responses $\mathbf{X}_i$.

It then follows from Bayes theorem that the posterior (i.e., constrained) distribution on the forcing response that is obtained after being updated with the observations $\mathbf{Y}_o$ has mean and variance-covariance matrix given by

$$\mu_{\mathbf{Y}|\mathbf{Y}_o} = \mu + \mathbf{\Sigma}_x \mathbf{H}'\left(\mathbf{H}\mathbf{\Sigma}_x\mathbf{H}' + \mathbf{\Sigma}_o\right)^{-1}\left(\mathbf{Y}_o - \mathbf{H}\mu\right) \tag{4}$$

$$\Sigma_{\mathbf{Y}|\mathbf{Y}_o} = \Sigma_x - \Sigma_x \mathbf{H}' \left(\mathbf{H} \Sigma_x \mathbf{H}' + \Sigma_o \right)^{-1} \mathbf{H} \Sigma_x \qquad (5)$$

Because $\mathbf{Y}$ and $\mathbf{X}_i$ span both the future and historical period, we may arrange their components as $\mu = \begin{bmatrix} \mu_f & \mu_h \end{bmatrix}$ and that $\Sigma_x = \begin{bmatrix} \Sigma_{x_f x_f} & \Sigma_{x_f x_h} \\ \Sigma_{x_h x_f} & \Sigma_{x_h x_h} \end{bmatrix}$, and for the future projection period, let $\mathbf{Y}_f = \mathbf{GY}$ where $\mathbf{G} = \begin{bmatrix} \mathbf{I}_f & \mathbf{0} \end{bmatrix}$. Then, we have

$$
\begin{aligned}
\widehat{\mathbf{Y}}_f^* &= \mathbf{G}\mu + \mathbf{G}\Sigma_x \mathbf{H}' \left(\mathbf{H}\Sigma_x \mathbf{H}' + \Sigma_o \right)^{-1} \left(\mathbf{Y}_o - \mathbf{H}\mu \right) \\
&= \mu_f + \Sigma_{x_f x_h} \left(\Sigma_{x_h x_h} + \Sigma_o \right)^{-1} \left(\mathbf{Y}_o - \mu_h \right)
\end{aligned} \qquad (6)
$$

$$
\begin{aligned}
\Sigma_{\widehat{\mathbf{Y}}_f^*|\mathbf{Y}_o} &= \mathbf{G}\Sigma_x \mathbf{G}' - \mathbf{G}\Sigma_x \mathbf{H}' \left(\mathbf{H}\Sigma_x \mathbf{H}' + \Sigma_o \right)^{-1} \mathbf{H}\Sigma_x \mathbf{G}' \\
&= \Sigma_{x_f x_f} - \Sigma_{x_f x_h} \left(\Sigma_{x_h x_h} + \Sigma_o \right)^{-1} \Sigma_{x_h x_f}
\end{aligned} \qquad (7)
$$

Note that in the special case where $\mathbf{Y}_o, \mathbf{Y}_f, \mu_h$, and μ_f are all scalars, representing key characteristics of time series, e.g., trends, then the future constrained projection reduces to

$$\widehat{Y}_f^* = \mu_f + \rho \frac{\sigma_{x_f} \sigma_{x_h}}{\sigma_{x_h}^2 + \sigma_o^2} \left(Y_o - \mu_h \right) \text{ and } \sigma_{\widehat{Y}_f^*|Y_o}^2 = \sigma_{x_f}^2 \left(1 - \frac{\rho^2}{1 + \sigma_o^2/\sigma_{x_h}^2} \right) (8)$$

which is the usual formulation of HEC method [equations 16 to 17 in Bowman *et al.* (*31*)] where μ_f and μ_h are multimodel ensemble mean values of the scalars in the future and historical periods, respectively, and σ_{x_f} and σ_{x_h} are the standard deviation of models; Y_o is the observed value and σ_o^2 is the variance of observational uncertainty; and ρ is the correlation coefficient derived from models describing the emergent relationship between the future conditions and the historical observable.

Implementation
Implementation of the method requires estimates of $\mathbf{Y}_o$, μ, Σ_o, and Σ_x.

1) The median value of the 200 HadCRUT5 realizations is taken as the best estimate of $\mathbf{Y}_o$ when using observations to constrain future projections. Individual model simulations are used as pseudo-observations when evaluating constraint performance using the imperfect model testing approach.

2) μ is estimated by averaging a sample of m model simulations, with the first run being selected from the collection of simulations available for each model. Each of those samples is smoothed with a natural cubic spline with 10 knots to filter out the effects of internal variability and short-duration natural forcing to the extent possible. The model that provides pseudo-observations for constraint performance evaluation is withheld when using the imperfect model testing approach.

3) Σ_o describes observational uncertainty due to measurement error and global mean surface temperature reconstruction on the one hand and internal variability on the other. The measurement and reconstruction error is estimated by calculating the variance-covariance matrix of the 200 HadCRUT5 realizations. We assume that internal variability in the observations is similar to that in

model-simulated global mean surface temperature. To estimate internal variability in the observations, we use simulations from CMIP6 models with more than one run (16 models in total) and follow these steps: (i) For each model, we obtain a sample of residual vectors by calculating the difference between each individual simulation and the model's ensemble mean. (ii) The regularized covariance matrix estimate based on these residuals is obtained using the Ledoit-Wolf (LW) estimator (*60, 61*). (iii) The resulting covariance matrices are averaged across all models to produce a multimodel mean covariance matrix representing internal variability, assuming the exchangeability of internal variability across models. The LW regularization ensures the invertibility of the variance-covariance matrix. We estimate the regularized matrix for each model separately to avoid giving disproportionate weight to models with larger ensemble sizes. The results are robust when compared to the approach that calculates a regularized covariance matrix from the combined sample of residual vectors from all models.

4) Σ_x, which describes variation in forced responses between models, is estimated from the collection of smoothed model series. As with the estimation of μ, the model providing the pseudo-observations is withheld from the estimation of Σ_x when performing imperfect model testing.

Imperfect model test
We evaluate the performance of constraint schemes in future 20-year periods with a lead time of 20 or 50 years using an imperfect model approach, where individual simulations of a model that is not used in developing the constraint are used as pseudo-observations. For this purpose, we use large ensemble simulations from three models that span the IPCC-assessed range of climate sensitivities (*57*). Individual historical simulations from these large ensembles serve as pseudo-observations to constrain the projections based on the remaining models, which are then compared with the future continuation of those historical simulations to evaluate the performance of the constraint. The only difference from the real-world application is that we assume no measurement uncertainty in the historical pseudo-observation.

Performance is evaluated on the basis of three factors: (i) the bias of the constrained projection, defined as the difference between future warming in the pseudo-observations and CMIP6-projected warming (or observation-constrained CMIP6 warming predictions); (ii) conditional uncertainty, represented by the 5th to 95th percentile uncertainty interval for each constrained projection calculated as the 90% confidence interval of the distribution; and (iii) unconditional uncertainty, represented by the range of constrained projections across different realizations of future pseudo-observations within a given large ensemble simulation. It is quantified as the RMSE when compared to the forced response of the corresponding large ensemble simulation.

The choice to use only one run per model to construct the prior distribution
The CMIP6 dataset is an ensemble of opportunity with different modeling centers producing varying number of realizations from their models. Different approaches can be used to combine these simulations to produce multimodel future projections.

One approach is to give each simulation equal weight, which is appealing because it allows for a large sample size, using all available simulations. However, this implicitly makes the very strong assumption that individual model simulations of global mean surface

temperature evolution are exchangeable, which is unlikely the case due to the wide range of climate sensitivities among models. Because some models have many more runs than others, this approach would disproportionately weight models with more simulations.

Another approach is to give one vote per model, which can be implemented in various ways. The most common method involves averaging all simulations within each model to derive its best estimate. The challenge here is that the contribution of internal variability to the best estimate depends heavily on the number of runs available for that model. For example, the influence of internal variability in a model with only one run would be similar to that in observations, while in a model with 50 runs, it would be only a small fraction of that in observations (~14% when measured by SD).

We therefore sought to ensure that internal variability affects all calculations uniformly. This can be done using a fixed number of runs per model. Using more than one run from each model would mean a smaller number of models could be included. Because model uncertainty is the main contributor to total uncertainty, we decided to prioritize the number of models and therefore chose to use only one run per model. This approach maximizes the information about model uncertainty, although it may reduce the information about the influence of internal variability. Nevertheless, given that the focus is on global mean surface temperature and that smoothing techniques are applied uniformly to remove internal variability from all runs, this approach was felt to be suitable for generating prior projections.

Masking with availability of observational data

When using historical observations to constrain future projections, we mask the model data to mimic the spatial and temporal availability of the observational data. This is done by first interpolating the model data onto a common $5° \times 5°$ grid. Grid boxes with missing values in the HadCRUT5 analysis are marked as missing in the model data for subsequent analysis.

Supplementary Materials
This PDF file includes:
Figs. S1 to S8
Table S1

REFERENCES AND NOTES

1. IPCC, "Summary for policymakers," in *Climate Change 2021: The Physical Science Basis. Contribution of Working Group I to the Sixth Assessment Report of the Intergovernmental Panel on Climate Change,* V. Masson-Delmotte, P. Zhai, A. Pirani, S. L. Connors, C. Péan, S. Berger, N. Caud, Y. Chen, L. Goldfarb, M. I. Gomis, M. Huang, K. Leitzell, E. Lonnoy, J. B. R. Matthews, T. K. Maycock, T. Waterfield, O. Yelekçi, R. Yu, B. Zhou, Eds. (Cambridge Univ. Press, 2021), pp. 3–32.

2. S. I. Seneviratne, X. Zhang, M. Adnan, W. Badi, C. Dereczynski, A. Di Luca, S. Ghosh, I. Iskandar, J. Kossin, S. Lewis, F. Otto, I. Pinto, M. Satoh, S. M. Vicente-Serrano, M. Wehner, B. Zhou, "Weather and Climate Extreme Events in a Changing Climate," in *Climate Change 2021: The Physical Science Basis. Contribution of Working Group I to the Sixth Assessment Report of the Intergovernmental Panel on Climate Change,* V. Masson-Delmotte, P. Zhai, A. Pirani, S. L. Connors, C. Péan, S. Berger, N. Caud, Y. Chen, L. Goldfarb, M. I. Gomis, M. Huang, K. Leitzell, E. Lonnoy, J. B. R. Matthews, T. K. Maycock, T. Waterfield, O. Yelekçi, R. Yu, B. Zhou, Eds. (Cambridge Univ. Press, 2021), pp. 1513–1766.

3. IPCC, *Climate Change 2021: The Physical Science Basis. Contribution of Working Group I to the Sixth Assessment Report of the Intergovernmental Panel on Climate Change* (Cambridge Univ. Press, 2021).

4. N. P. Gillett, Halving of the uncertainty in projected warming over the past decade. *npj Clim. Atmos. Sci.* **7**, 146 (2024).

5. K. Eisenack, M. Paschen, Adapting long-lived investments under climate change uncertainty. *J. Environ. Econ. Manag.* **116**, 102743 (2022).

6. ASCE, *Adapting Infrastructure and Civil Engineering Practice to a Changing Climate,* J. R. Olsen, Ed. (American Society of Civil Engineers, 2015).

7. V. Eyring, S. Bony, G. A. Meehl, C. A. Senior, B. Stevens, R. J. Stouffer, K. E. Taylor, Overview of the Coupled Model Intercomparison Project Phase 6 (CMIP6) experimental design and organization. *Geosci. Model Dev.* **9**, 1937–1958 (2016).

8. K. E. Taylor, R. J. Stouffer, G. A. Meehl, An overview of CMIP5 and the experiment design. *Bull. Am. Meteorol. Soc.* **93**, 485–498 (2012).

9. H. Le Treut, R. Somerville, U. Cubasch, Y. Ding, C. Mauritzen, A. Mokssit, T. Peterson, M. Prather, "Historical overview of climate change," in *Climate Change 2007: The Physical Science Basis. Contribution of Working Group I to the Fourth Assessment Report of the Intergovernmental Panel on Climate Change,* S. Solomon, D. Qin, M. Manning, Z. Chen, M. Marquis, K. B. Averyt, M. Tignor, H. L. Miller, Eds. (Cambridge Univ. Press, 2007) pp. 94–127.

10. U. Cubasch, D. Wuebbles, D. Chen, M. C. Facchini, D. Frame, N. Mahowald, J.-G. Winther, "Introduction," in *Climate Change 2013: The Physical Science Basis. Contribution of Working Group I to the Fifth Assessment Report of the Intergovernmental Panel on Climate Change,* T. F. Stocker, D. Qin, G.-K. Plattner, M. Tignor, S. K. Allen, J. Boschung, A. Nauels, Y. Xia, V. Bex, P. M. Midgley, Eds. (Cambridge Univ. Press, 2013) pp. 119–158.

11. E. Hawkins, R. Sutton, The potential to narrow uncertainty in regional climate predictions. *Bull. Am. Meteorol. Soc.* **90**, 1095–1108 (2009).

12. D. Chen, M. Rojas, B. H. Samset, K. Cobb, A. Diongue Niang, P. Edwards, S. Emori, S. H. Faria, E. Hawkins, P. Hope, P. Huybrechts, M. Meinshausen, S. K. Mustafa, G. K. Plattner, A. M. Tréguier, "Framing, context, and methods supplementary material," in *Climate Change 2021: The Physical Science Basis. Contribution of Working Group I to the Sixth Assessment Report of the Intergovernmental Panel on Climate Change,* V. Masson-Delmotte, P. Zhai, A. Pirani, S. L. Connors, C. Péan, S. Berger, N. Caud, Y. Chen, L. Goldfarb, M. I. Gomis, M. Huang, K. Leitzell, E. Lonnoy, J. B. R. Matthews, T. K. Maycock, T. Waterfield, O. Yelekçi, R. Yu, B. Zhou, Eds. (Cambridge Univ. Press, 2021) pp. 147–280.

13. Z. Hausfather, H. F. Drake, T. Abbott, G. A. Schmidt, Evaluating the performance of past climate model projections. *Geophys. Res. Lett.* **47**, e2019GL085378 (2020).

14. P. A. Stott, J. A. Kettleborough, Origins and estimates of uncertainty in predictions of twenty-first century temperature rise. *Nature* **416**, 723–726 (2002).

15. P. A. Stott, J. F. B. Mitchell, M. R. Allen, T. L. Delworth, J. M. Gregory, G. A. Meehl, B. D. Santer, Observational constraints on past attributable warming and predictions of future global warming. *J. Climate* **19**, 3055–3069 (2006).

16. T. C. K. Lee, F. W. Zwiers, X. Zhang, M. Tsao, Evidence of decadal climate prediction skill resulting from changes in anthropogenic forcing. *J. Climate* **19**, 5305–5318 (2006).

17. K. B. Tokarska, M. B. Stolpe, S. Sippel, E. M. Fischer, C. J. Smith, F. Lehner, R. Knutti, Past warming trend constrains future warming in CMIP6 models. *Sci. Adv.* **6**, eaaz9549 (2020).

18. H. Shiogama, M. Watanabe, H. Kim, N. Hirota, Emergent constraints on future precipitation changes. *Nature* **602**, 612–616 (2022).

19. L. Brunner, A. G. Pendergrass, F. Lehner, A. L. Merrifield, R. Lorenz, R. Knutti, Reduced global warming from CMIP6 projections when weighting models by performance and independence. *Earth Syst. Dynam.* **11**, 995–1012 (2020).

20. R. Knutti, M. R. Allen, P. Friedlingstein, J. M. Gregory, G. C. Hegerl, G. A. Meehl, M. Meinshausen, J. M. Murphy, G. K. Plattner, S. C. B. Raper, T. F. Stocker, P. A. Stott, H. Teng, T. M. L. Wigley, A review of uncertainties in global temperature projections over the twenty-first century. *J. Climate* **21**, 2651–2663 (2008).

21. D. Jiménez-de-la-Cuesta, T. Mauritsen, Emergent constraints on Earth's transient and equilibrium response to doubled CO_2 from post-1970s global warming. *Nat. Geosci.* **12**, 902–905 (2019).

22. J. T. Kiehl, Twentieth century climate model response and climate sensitivity. *Geophys. Res. Lett.* **34**, L22710 (2007).

23. J. Y. Lee, J. Marotzke, G. Bala, L. Cao, S. Corti, J. P. Dunne, F. Engelbrecht, E. Fischer, J. C. Fyfe, C. Jones, A. Maycock, J. Mutemi, O. Ndiaye, S. Panickal, T. Zhou, "Future global climate: Scenario-based projections and near-term information," in *Climate Change 2021: The Physical Science Basis. Contribution of Working Group I to the Sixth Assessment Report of the Intergovernmental Panel on Climate Change,* V. Masson-Delmotte, P. Zhai, A. Pirani, S. L. Connors, C. Péan, S. Berger, N. Caud, Y. Chen, L. Goldfarb, M. I. Gomis, M. Huang, K. Leitzell, E. Lonnoy, J. B. R. Matthews, T. K. Maycock, T. Waterfield, O. Yelekçi, R. Yu, B. Zhou, Eds. (Cambridge Univ. Press, 2021), pp. 553–672.

24. Y. Liang, N. P. Gillett, A. H. Monahan, Climate model projections of 21st century global warming constrained using the observed warming trend. *Geophys. Res. Lett.* **47**, e2019GL086757 (2020).

25. A. Ribes, S. Qasmi, N. P. Gillett, Making climate projections conditional on historical observations. *Sci. Adv.* **7**, eabc0671 (2021).

26. S. C. Sherwood, M. J. Webb, J. D. Annan, K. C. Armour, P. M. Forster, J. C. Hargreaves, G. Hegerl, S. A. Klein, K. D. Marvel, E. J. Rohling, M. Watanabe, T. Andrews, P. Braconnot, C. S. Bretherton, G. L. Foster, Z. Hausfather, A. S. von der Heydt, R. Knutti, T. Mauritsen, J. R. Norris, C. Proistosescu, G. A. Schmidt, K. B. Tokarska, M. D. Zelinka, An assessment of Earth's climate sensitivity using multiple lines of evidence. *Rev. Geophys.* **58**, e2019RG000678 (2020).

27. M. Schlund, A. Lauer, P. Gentine, S. C. Sherwood, V. Eyring, Emergent constraints on equilibrium climate sensitivity in CMIP5: Do they hold for CMIP6? *Earth Syst. Dynam.* **11**, 1233–1258 (2020).

28. F. Brient, T. Schneider, Z. Tan, S. Bony, X. Qu, A. Hall, Shallowness of tropical low clouds as a predictor of climate models' response to warming. *Climate Dynam.* **47**, 433–449 (2015).

29. A. Hall, X. Qu, Using the current seasonal cycle to constrain snow albedo feedback in future climate change. *Geophys. Res. Lett.* **33**, L03502 (2006).

30. X. Qu, A. Hall, On the persistent spread in snow-albedo feedback. *Climate Dynam.* **42**, 69–81 (2014).

31. K. W. Bowman, N. Cressie, X. Qu, A. Hall, A hierarchical statistical framework for emergent constraints: Application to snow-albedo feedback. *Geophys. Res. Lett.* **45**, 13050–13059 (2018).

32. C. Li, Q. Sun, J. Wang, Y. Liang, F. W. Zwiers, X. Zhang, T. Li, Constraining projected changes in rare intense precipitation events across global land regions. *Geophys. Res. Lett.* **51**, e2023GL105605 (2024).

33. Z. Chen, T. Zhou, X. Chen, W. Zhang, M. Zuo, W. Man, Y. Qian, Emergent constrained projections of mean and extreme warming in China. *Geophys. Res. Lett.* **50**, 13050–13059 (2023).

34. A. Ribes, J. Boé, S. Qasmi, B. Dubuisson, H. Douville, L. Terray, An updated assessment of past and future warming over France based on a regional observational constraint. *Earth Syst. Dynam.* **13**, 1397–1415 (2022).

35. S. Qasmi, A. Ribes, Reducing uncertainty in local temperature projections. *Sci. Adv.* **8**, eabo6872 (2022).

36. G. J. Boer, D. M. Smith, C. Cassou, F. Doblas-Reyes, G. Danabasoglu, B. Kirtman, Y. Kushnir, M. Kimoto, G. A. Meehl, R. Msadek, W. A. Mueller, K. E. Taylor, F. Zwiers, M. Rixen, Y. Ruprich-Robert, R. Eade, The Decadal Climate Prediction Project (DCPP) contribution to CMIP6. *Geosci. Model Dev.* **9**, 3751–3777 (2016).

37. P. M. Cox, C. Huntingford, M. S. Williamson, Emergent constraint on equilibrium climate sensitivity from global temperature variability. *Nature* **553**, 319–322 (2018).

38. A. Hall, P. Cox, C. Huntingford, S. Klein, Progressing emergent constraints on future climate change. *Nat. Clim. Change* **9**, 269–278 (2019).

39. J. D. Herman, J. D. Quinn, S. Steinschneider, M. Giuliani, S. Fletcher, Climate adaptation as a control problem: Review and perspectives on dynamic water resources planning under uncertainty. *Water Resour. Res.* **56**, e24389 (2020).

40. H. Shiogama, H. Tatebe, M. Hayashi, M. Abe, M. Arai, H. Koyama, Y. Imada, Y. Kosaka, T. Ogura, M. Watanabe, MIROC6 Large Ensemble (MIROC6-LE): Experimental design and initial analyses. *Earth Syst. Dynam.* **14**, 1107–1124 (2023).

41. T. Ziehn, M. A. Chamberlain, R. M. Law, A. Lenton, R. W. Bodman, M. Dix, L. Stevens, Y.-P. Wang, J. Srbinovsky, The Australian Earth system model: ACCESS-ESM1.5. *J. South. Hemisph. Earth Syst. Sci.* **70**, 193–214 (2020).

42. N. C. Swart, J. N. S. Cole, V. V. Kharin, M. Lazare, J. F. Scinocca, N. P. Gillett, J. Anstey, V. Arora, J. R. Christian, S. Hanna, Y. Jiao, W. G. Lee, F. Majaess, O. A. Saenko, C. Seiler, C. Seinen, A. Shao, M. Sigmond, L. Solheim, K. von Salzen, D. Yang, B. Winter, The Canadian Earth System Model version 5 (CanESM5.0.3). *Geosci. Model Dev.* **12**, 4823–4873 (2019).

43. G. C. Hegerl, S. Brönnimann, T. Cowan, A. R. Friedman, E. Hawkins, C. Iles, W. Müller, A. Schurer, S. Undorf, Causes of climate change over the historical record. *Environ. Res. Lett.* **14**, 123006 (2019).

44. Y. H. Kim, S. K. Min, N. P. Gillett, D. Notz, E. Malinina, Observationally-constrained projections of an ice-free Arctic even under a low emission scenario. *Nat. Commun.* **14**, 3139 (2023).

45. M. G. Donat, R. Mahmood, P. Cos, P. Ortega, F. Doblas-Reyes, Improving the forecast quality of near-term climate projections by constraining internal variability based on decadal predictions and observations. *Environ. Res. Climate* **3**, 035013 (2024).

46. Y. Liang, N. P. Gillett, A. H. Monahan, Accounting for Pacific climate variability increases projected global warming. *Nat. Clim. Change* **14**, 608–614 (2024).

47. P. Dai, J. Nie, Y. Yu, R. Wu, Constraints on regional projections of mean and extreme precipitation under warming. *Proc. Natl. Acad. Sci. U.S.A.* **121**, e2312400121 (2024).

48. Z. Chen, T. Zhou, X. Chen, W. Zhang, L. Zhang, M. Wu, L. Zou, Observationally constrained projection of Afro-Asian monsoon precipitation. *Nat. Commun.* **13**, 2552 (2022).

49. J. Hansen, M. Sato, P. Kharecha, K. von Schuckmann, Earth's energy imbalance and implications. *Atmos. Chem. Phys.* **11**, 13421–13449 (2011).

50. P. T. Brown, K. Caldeira, Greater future global warming inferred from Earth's recent energy budget. *Nature* **552**, 45–50 (2017).

51. G. H. Roe, M. B. Baker, The shape of things to come: Why is climate change so predictable? *J. Climate* **22**, 4574–4589 (2009).

52. IPCC, *Climate Change 2001: The Scientific Basis. Contribution of Working Group I to the Third Assessment Report of the Intergovernmental Panel on Climate Change* (Cambridge Univ. Press, 2001), vol. 881.

53. N. Maher, S. B. Power, J. Marotzke, More accurate quantification of model-to-model agreement in externally forced climatic responses over the coming century. *Nat. Commun.* **12**, 788 (2021).

54. R. C. J. Wills, D. S. Battisti, K. C. Armour, T. Schneider, C. Deser, Pattern recognition methods to separate forced responses from internal variability in climate model ensembles and observations. *J. Climate* **33**, 8693–8719 (2020).

55. Y. Liang, N. P. Gillett, A. H. Monahan, Emergent constraints on CMIP6 climate warming projections: Contrasting cloud- and surface temperature–based constraints. *J. Climate* **35**, 1809–1824 (2022).

56. F. Brient, T. Schneider, Constraints on climate sensitivity from space-based measurements of low-cloud reflection. *J. Climate* **29**, 5821–5835 (2016).

57. C. Smith, Z. R. J. Nicholls, K. Armour, W. Collins, P. Forster, M. Meinshausen, M. D. Palmer, M. Watanabe, "The Earth's energy budget, climate feedbacks, and climate sensitivity supplementary material," in *Climate Change 2021: The Physical Science Basis. Contribution of Working Group I to the Sixth Assessment Report of the Intergovernmental Panel on Climate Change*, V. Masson–Delmotte, P. Zhai, A. Pirani, S. L. Connors, C. Péan, S. Berger, N. Caud, Y. Chen, L. Goldfarb, M. I. Gomis, M. Huang, K. Leitzell, E. Lonnoy, J. B. R. Matthews, T. K. Maycock, T. Waterfield, O. Yelekçi, R. Yu, B. Zhou, Eds. (Cambridge Univ. Press, 2021); https://www.ipcc.ch/report/ar6/wg1/downloads/report/IPCC_AR6_WGI_Chapter07_SM.pdf.

58. C. P. Morice, J. J. Kennedy, N. A. Rayner, J. P. Winn, E. Hogan, R. E. Killick, R. J. H. Dunn, T. J. Osborn, P. D. Jones, I. R. Simpson, An updated assessment of near-surface temperature change from 1850: The HadCRUT5 data set. *J. Geophys. Res. Atmos.* **126**, e2019JD032361 (2021).

59. H. Douville, S. Qasmi, A. Ribes, O. Bock, Global warming at near-constant tropospheric relative humidity is supported by observations. *Commun. Earth Environ.* **3**, 237 (2022).

60. O. Ledoit, M. Wolf, A well-conditioned estimator for large-dimensional covariance matrices. *J. Multivar. Anal.* **88**, 365–411 (2004).

61. A. Ribes, S. Planton, L. Terray, Application of regularised optimal fingerprinting to attribution. Part I: Method, properties and idealised analysis. *Climate Dynam.* **41**, 2817–2836 (2013).

62. G. A. Meehl, C. A. Senior, V. Eyring, G. Flato, J.-F. Lamarque, R. J. Stouffer, K. E. Taylor, M. Schlund, Context for interpreting equilibrium climate sensitivity and transient climate response from the CMIP6 Earth system models. *Sci. Adv.* **6**, eaba1981 (2020).